Universidade do Minho
Escola de Engenharia

International Masonry Society

9th International Masonry Conference 2014 in Guimarães

Homogenized non-linear dynamic model for masonry walls in two-way bending

MILANI, GABRIELE[1]; LOURENÇO, PAULO[2]

ABSTRACT: A simple homogenization approach accounting for mortar joint damaging is presented, suitable to analyse entire panels in two-way bending in the non-linear dynamic field. A rectangular running bond elementary cell (RVE) is subdivided into several layers along the thickness and, for each layer, a discretization where bricks are meshed with plane-stress three-noded triangular elements and joints are reduced to interfaces with damaging behaviour is assumed. Non linearity is due exclusively to joints cracking, which exhibit also a frictional behaviour with limited tensile and compressive strength with softening. A damaging material is utilized for joints in order to properly take into account the actual opening and closure of cracked mortar under cyclic loads. Finally, macroscopic curvature bending moment diagrams are obtained integrating along the thickness in-plane micro-stresses of each layer.

Homogenized masonry flexural response under load-unload conditions is then implemented at a structural level in a FE non-linear code based on a discretization with rigid three-noded elements and elasto-damaging interfaces where elastic and inelastic deformation is allowed only for flexural actions. The two step model proposed is validated both at a cell and structural level, comparing results obtained with both experimental data and existing macroscopic numerical approaches available in the literature.

Keywords: *masonry, non-linear dynamic analysis, homogenization*

1 INTRODUCTION

The out-of-plane weakness is a quite common feature for masonry structures [3][4] and is due to several factors, among the most important is the relatively low tensile resistance of the mortar joint. Earthquake damage surveys have demonstrated that the lack of out-of-plane strength is a primary cause of failure in most traditional forms of masonry construction. This fact is confirmed in the case of old masonry monuments for which the thickness of façades is often relatively small with respect to the other dimensions.

Despite renewed research efforts, a number of difficulties still remain for the numerical analysis of masonry structures, especially in modelling their constitutive behaviour at a structural level, whose salient characteristics include heterogeneity, orthotropy, different responses under tension and compression and softening behaviour. At present, it can be affirmed that still the most effective strategy for the analysis of large masonry walls in the non-linear range [5] is the so called macro-

[1)] Assistant Professor, Technical University of Milan, Piazza Leonardo da Vinci 32, 20133 Milan, Italy, gabriele.milani@polimi.it
[2)] Full Professor, University of Minho, Campus de Azurem, Guimaraes, Portugal, pbl@civil.uminho.pt

modelling approach. In addition, it must be noted that dynamic analyses are probably the most suited numerical approach to predict both the actual strength of single walls and the damage induced by an earthquake excitation.

In this context, the determination of the macroscopic mechanical properties to be utilized is a key but tricky issue. To properly take into account masonry orthotropic behaviour in the inelastic range, it is possible to use micro-modelling [6], macro-modelling [7], or homogenization [8]-[10]. The typical need of micro-modelling of a distinct representation of blocks and mortar makes its application prohibitive for large scale structures [11] and hence more suited for small specimens and single structural elements. For large scale simulations, homogenization could be rather useful, by accounting the complex geometry of the basic cell and the constituent material properties only at the meso-scale.

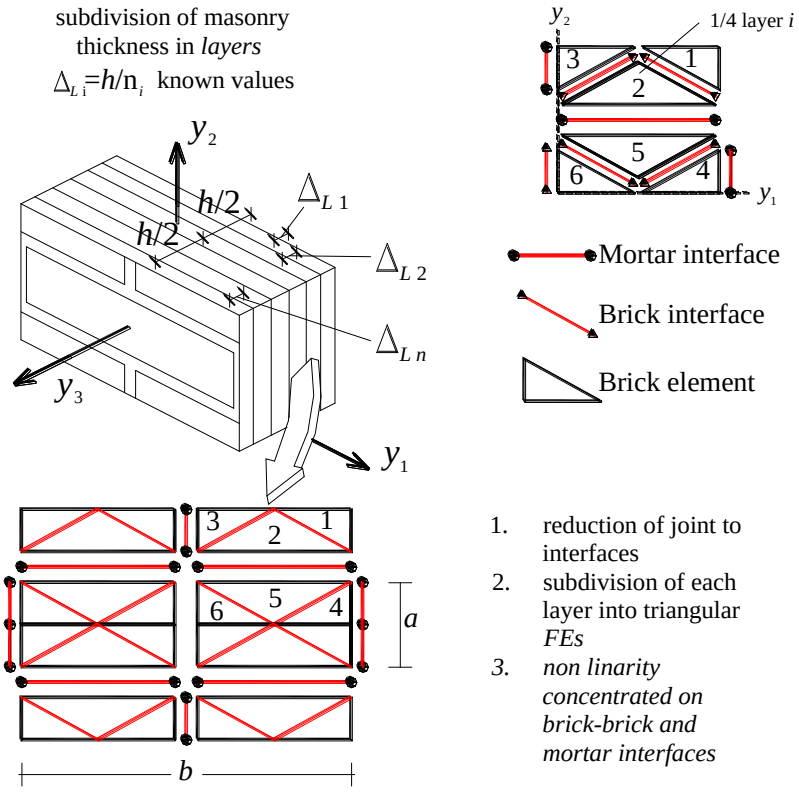

Figure 1: The micro-mechanical model used to determine macroscopic masonry behaviour.

At the macro-scale, the approach here presented is founded on the hypothesis that in many cases the seismic damage of masonry monuments can be investigated by considering their architectural parts as separate, i.e. subdividing the structure into “macro-elements” [4]. As a matter of fact, for simple façades (i.e. without significant variations of thickness) the slenderness (intended as the ratio between height and thickness) is often relatively high and failures tend to occur with the developing of cylindrical yield lines.

In the present work, attention is focused on the out-of-plane behaviour of this masonry walls, so that a Kirchhoff-Love approach is suitable for the description of its behaviour under dynamic loads. The model assumes a discretization with Munro and Da Fonseca [12] triangular rigid infinitely resistant elements connected by inelastic flexural interfaces exhibiting softening and damage. Mechanical properties of the interfaces are suitably deduced from a recently presented homogenization procedure in the inelastic range.

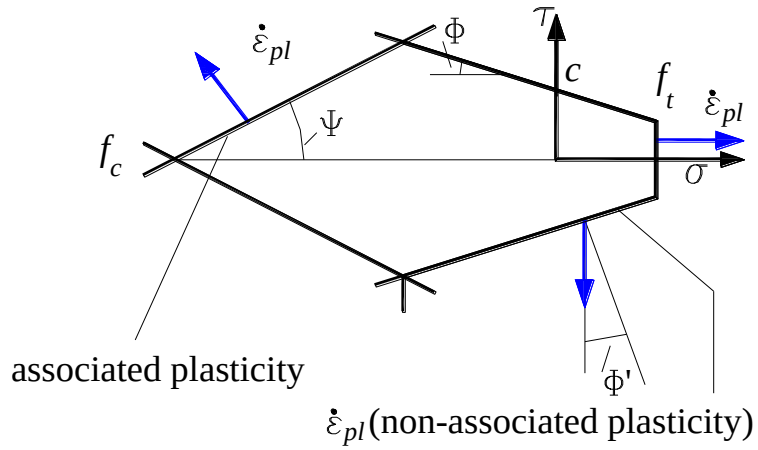

Figure 2: Modified Mohr–Coulomb criterion for the mortar joint/mortar–brick interface.

2 HOMOGENIZATION

The homogenization model is based on the identification of an elementary cell or Representative Element of Volume (REV) constituted by elastic blocks and joints reduced to interface with a homogeneous plate [13].

The representative element of volume *Y* (RVE or elementary cell) depicted in Figure 1 is considered. *Y* contains all the information necessary for describing completely the macroscopic behaviour of an entire wall. Homogenization consists in introducing averaged quantities for macroscopic strain and stress tensors ($\mathbf{E}$ and $\mathbf{\Sigma}$), as follows:

$$\begin{aligned} \mathbf{E} &= <\boldsymbol{\varepsilon}> = \frac{1}{A}\int_Y \boldsymbol{\varepsilon}(\mathbf{u})dY \\ \mathbf{\Sigma} &= <\boldsymbol{\sigma}> = \frac{1}{A}\int_Y \boldsymbol{\sigma}dY\,, \end{aligned} \qquad (1)$$

where *A* stands for the area of the elementary cell, $\boldsymbol{\varepsilon}$ and $\boldsymbol{\sigma}$ stand for the local quantities and <*> is the average.

Periodicity conditions are imposed on the stress field $\boldsymbol{\sigma}$ and the displacement field **u**, so that:

$$\begin{cases} \mathbf{u} = \mathbf{E}\mathbf{y} + \mathbf{u}^{\text{per}} \quad \mathbf{u}^{\text{per}} \text{ on } \partial Y \\ \boldsymbol{\sigma}\mathbf{n} \quad \text{anti-periodic} \quad \text{on } \partial Y \end{cases} \qquad (2)$$

where $\mathbf{u}^{\text{per}}$ stands for a periodic displacement field.

In the model, joints are reduced to interfaces with zero thickness and bricks are discretized by means of a coarse mesh constituted by plane-stress elastic triangles, Figure 1. All the non-linearity in the RVE is concentrated exclusively on interfaces between adjoining elements both on brick and joint.

The elastic domain of joints is bounded by a composite yield surface that includes tension, shear and compression failure with softening (see Figure 2). A multi-surface plasticity model is adopted, with softening in both tension and compression. The parameters f_t and f_c are, respectively, the tensile and compressive Mode-I strength of the mortar or mortar–brick interfaces, *c* is the cohesion, Φ is the friction angle, and Ψ is the angle which defines the linear compression cap.

The usual elasto-plastic equations for single surface plasticity hold; assuming the hypothesis of small deformations, the total strain rate $\dot{\boldsymbol{\varepsilon}}$ is decomposed into an elastic component $\dot{\boldsymbol{\varepsilon}}_{el}$ and a plastic component $\dot{\boldsymbol{\varepsilon}}_{pl}$. The elastic strain rate is related to the stress rate by the elastic constitutive matrix **D** as $\dot{\boldsymbol{\sigma}} = \mathbf{D}\dot{\boldsymbol{\varepsilon}}_{el}$ whereas the non-associated plasticity assumption allows to link $\dot{\boldsymbol{\varepsilon}}_{pl}$ with $\dot{\lambda}_i$ as

$\dot{\boldsymbol{\varepsilon}}_{pl} = \lambda_i \partial g_i / \partial \boldsymbol{\sigma}$ where g_i is the plastic potential corresponding to the i-th yield surface (which rules the direction of $\dot{\boldsymbol{\varepsilon}}_{pl}$ in the stress space) and $\boldsymbol{\sigma} = \begin{bmatrix} \sigma & \tau \end{bmatrix}^T$. In classic non-associated plasticity g_i may not coincide with f_i.

For the tension mode, exponential softening on the tensile strength is assumed according to the mode I experiments by many authors. The yield function reads:

$$f_1(\boldsymbol{\sigma}, \kappa_1) = \sigma - f_t(\kappa_1) \quad (3)$$

where the yield value $f_t(\kappa_1)$ deteriorates in agreement with the following formula:

$$f_t(\kappa_1) = f_{t0} e^{-\frac{f_{t0}}{G_f^I}\kappa_1} \quad (4)$$

where f_{t0} is the initial joint tensile strength and G_f^I is the mode I fracture energy. An associated flow rule is assumed here.

When dealing with the shear mode, a Mohr-Coulomb yield function is adopted:

$$f_2(\boldsymbol{\sigma}, \kappa_2) = |\tau| + \sigma \tan\phi(\kappa_2) - c(\kappa_2) \quad (5)$$

where the yield values c and $\tan\phi$ are ruled by the following formulas:

$$c(\kappa_2) = c_0 e^{-\frac{c_0}{G_f^{II}}\kappa_2}$$
$$\tan\phi = \tan\phi_0 + (\tan\phi_r - \tan\phi_0)(c_0 - c)/c_0 \quad (6)$$

being c_0 and $\tan\phi_0$ the initial cohesion and friction angle, G_f^{II} is the mode II fracture energy and $\tan\phi_r$ is the residual friction angle. A non-associated flow rule is assumed here, with $g_2 = |\tau|$.

When dealing with the linearized compressive cap, an associated elastic-perfectly plastic behaviour is assumed, with the yield function expressed by:

$$f_3(\boldsymbol{\sigma}) = |\tau| + (\sigma + f_c)\tan\vartheta \quad (7)$$

where f_c is the uniaxial compressive strength.

The response of the RVE under out-of-plane actions is obtained subdividing along the thickness the unit cell into several layers (typically 20). A displacement driven approach is adopted, meaning that macroscopic curvature increments $\Delta\chi_{11}$, $\Delta\chi_{22}$ and $\Delta\chi_{12}$ are applied through suitable periodic boundary displacement increments. Thus each layer undergoes only in-plane displacements and may be modelled through plane stress FEs. Bending moments and torsion are finally obtained at each step simply by integration along the thickness of the quantity $\boldsymbol{\sigma}\ y_3$:

$$\mathbf{M} = <\boldsymbol{\sigma} y_3> = \frac{1}{A}\int_Y \boldsymbol{\sigma} y_3 dY \quad (8)$$

For the macroscopic dynamic nonlinear analyses, the elasto-plastic unloading behaviour would be not realistic. For this reason, the unloading rule is assumed as the material was a damaging one, i.e. there is a decrease of the stiffness.

3 NON LINEAR MASONRY FLEXURAL BEHAVIOUR AT DIFFERENT ORIENTATION OF THE BED JOINT WITH RESPECT TO MATERIAL AXIS

Some experimental information regarding crack pattern and moment-curvature diagrams for clay brick masonry in flexion and in absence of pre-compression is available from van der Pluijm [14][15]. In particular, the flexural behaviour of several small panels in four point bending with the bed joints making a variable angle ϑ with the direction of loading were experimentally tested.

For the experimentation, standard Dutch bricks of dimensions 200×52×100 mm^3 with 10 mm thick mortar joints were used. Mechanical properties of the constituent materials are summarized in Table 1 and are taken, where possible, in agreement with average experimental values available for constituent materials.

Three directions are here investigated, namely ϑ=0° (vertical bending), ϑ=30° (inclined bending), ϑ=90° (horizontal bending). For all experimentally tested wallettes, both the elastic limit and the peak resistance point in the curvature-bending moment diagram are available from the literature. On the contrary, no information is given on the post-peak branch (softening) and on the effect of vertical compressive loads on the flexural behaviour.

A full comparison between experimental data and numerical model response is summarized in Figure 3. While the orthotropy at failure is somewhat evident, the dispersion of experimental data does not allow estimating the typical anisotropy exhibited by masonry in the elastic range.

Table 1: [14][15] experimental data. Mechanical properties assumed for the constituent materials.

	joint	brick-brick interface	Triangles brick		
E	4000	11000	11000	[MPa]	Young Modulus
G	2000	5500	5500	[MPa]	Shear Modulus
c	1.8 ft	1	-	[MPa]	Cohesion
f_t	0.3	-	-	[MPa]	Tensile strength
f_c	20	-	-	[MPa]	Compressive strength
Φ	30	45	-	[°]	Friction angle
Ψ	45	-	-	[°]	Angle of the linearized compressive cap
G_f^I	0.018	10	-	[N/mm]	Mode I fracture energy
G_f^{II}	0.022	10	-	[N/mm]	Mode II fracture energy

4 STRUCTURAL NON-LINEAR DYNAMIC PROBLEM

The finite element model utilized next for the non-linear analysis of masonry panes out-of-plane loaded is based on the triangular element proposed by Munro and Da Fonseca [12] and seems perfectly suited to solve in a simple way the dynamic problem, since elastic-plastic deformation is concentrated only at the interfaces between adjoining elements and is due exclusively to bending moment. The displacement field is assumed linear inside each element and nodal velocities are taken as optimization variables. Denoting with $\mathbf{w}_E = \begin{bmatrix} w_i^E & w_j^E & w_k^E \end{bmatrix}^T$ element E nodal velocities and with $\boldsymbol{\theta}_E = \begin{bmatrix} \vartheta_i^E & \vartheta_j^E & \vartheta_k^E \end{bmatrix}^T$ side normal rotations, $\boldsymbol{\theta}_E$ and $\mathbf{w}_E$ are linked by the compatibility equation (Figure 4-a and –b):

$$\boldsymbol{\theta}_E = \mathbf{B}_E \mathbf{w}_E$$

$$\mathbf{B}_E = \frac{1}{2A_E} \begin{bmatrix} \frac{b_i b_i + c_i c_i}{l_i} & \frac{b_i b_j + c_i c_j}{l_i} & \frac{b_i b_k + c_i c_k}{l_i} \\ \frac{b_j b_i + c_j c_i}{l_j} & \frac{b_j b_j + c_j c_j}{l_j} & \frac{b_j b_k + c_j c_k}{l_j} \\ \frac{b_k b_i + c_k c_i}{l_k} & \frac{b_k b_j + c_k c_j}{l_k} & \frac{b_k b_k + c_k c_k}{l_k} \end{bmatrix} \quad (9)$$

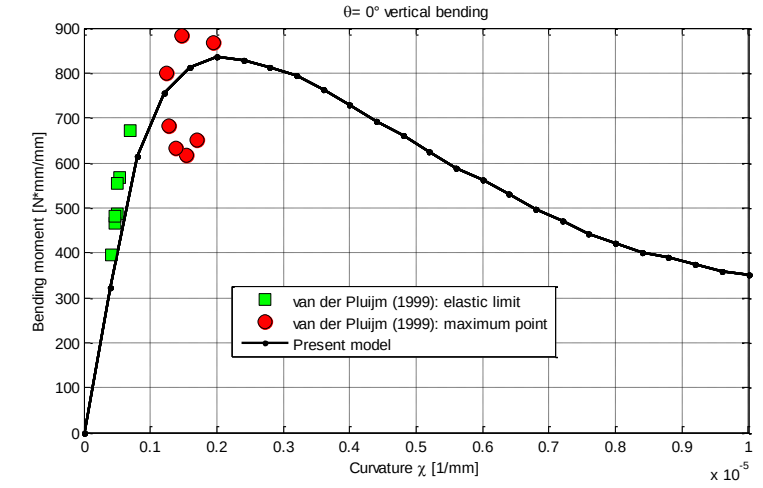

-a

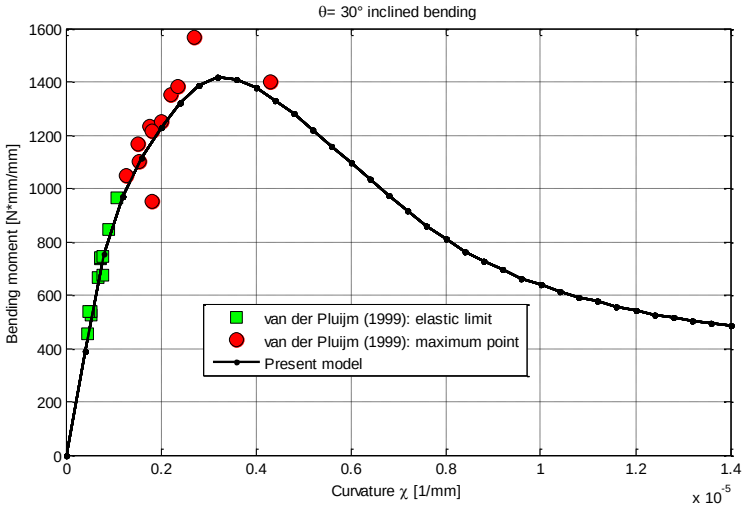

-b

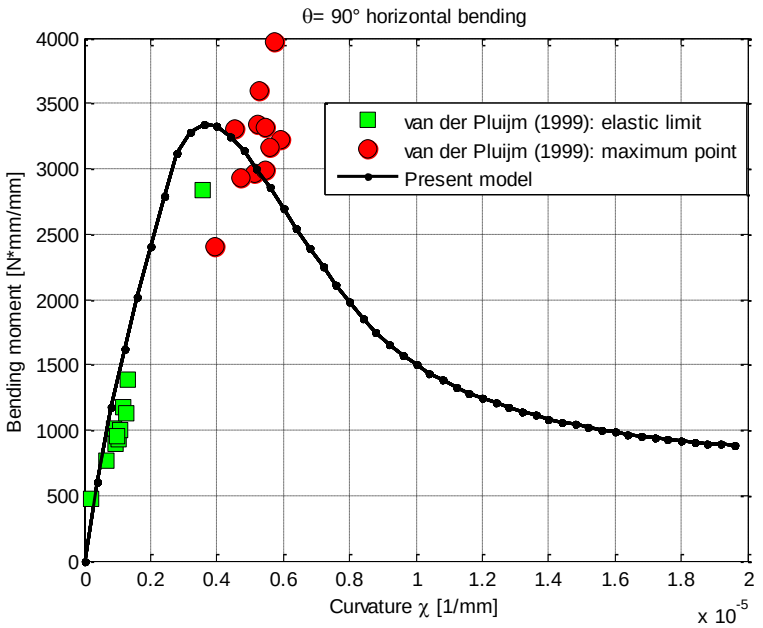

-c

Figure 3: Simulations at cell level. [14][15] experimental data. Bending moment-curvature diagrams at different orientations of the bending moment/horizontal joint. -a: 0°. -b: 30°. -c: 90°.

with $b_i = y_j - y_k$, $c_i = x_k - x_j$ ad A_E element area. Due to the linear interpolation of displacements perpendicular to the plate middle plane, elastic deformation and plastic dissipation occurs only along each interface I between two adjacent triangles R and K or on a boundary side B of an element Q (see Figure 4-c). Internal work W_I^{in} stored in each interface I can be written as follows:

$$\begin{aligned} W_I^{in} &= M_{nn,I}^{+} \vartheta_I \quad \vartheta_I > 0 \\ W_I^{in} &= M_{nn,I}^{-} \left|\vartheta_I\right| \quad \vartheta_I < 0 \end{aligned} \qquad (10)$$

Where $\vartheta_I = \vartheta_i^R + \vartheta_j^K$ is the relative rotation between R and K along I (see Figure 4-b) and $M_{nn,I}^{+}$ and $M_{nn,I}^{-}$ are positive and negative bending moments along I.

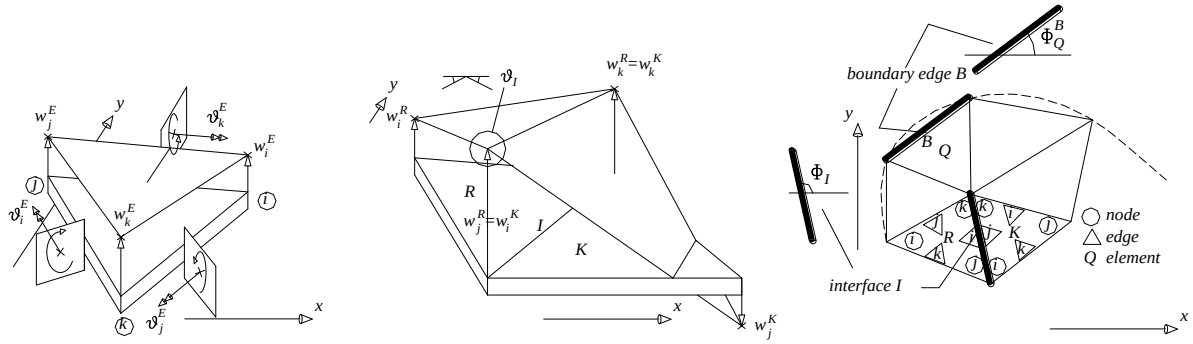

-a -b -c

Figure 4: Triangular plate element used for the FE non-linear analyses (-a), rotation along an interface between adjacent triangles (-b), discretization of the 2D domain (-c).

The time integration scheme is a classic Newmark approach where the dynamic equilibrium equation is written node by node.

Translational equilibrium equation along the perpendicular direction of an element E reads as follows:

$$m_i \ddot{U}_i + \xi_i \dot{U}_i + K_i U_i = F_i \qquad (11)$$

Where F_i is the force acting on node *I*, m_i, ξ_i and K_i are mass, damping and stiffness, $\ddot{U}_i$, $\dot{U}_i$ and U_i are acceleration, velocity and displacement of the node.

Each single nodal equation may be properly assembled into a global matrix formulation. In particular, remembering that:

$$\begin{aligned} \boldsymbol{\theta}_E &= \mathbf{B}_E \mathbf{U}_E \\ -\mathbf{R}_E &= \mathbf{B}_E^T \mathbf{M}_E \end{aligned} \qquad (12)$$

Where we indicate with $\boldsymbol{\theta}_E$ the edge rotations matrix and with $\mathbf{R}_E$ the out-of-plane forces applied on vertexes of the element which maintain the element in equilibrium.

Considering the non-linear relationship between $\mathbf{M}_E$ and $\boldsymbol{\theta}_E$ in the form $\mathbf{M}_E = \mathbf{K}_E(t)\boldsymbol{\theta}_E$, the previous equations may be re-written as:

$$-\mathbf{R}_E = \mathbf{B}_E^T \mathbf{K}_E(t) \mathbf{B}_E \mathbf{U}_E \qquad (13)$$

The contribution to the three nodes belonging to an element E of the single element is:

$$\mathbf{m}_E \ddot{\mathbf{U}}_E + \boldsymbol{\xi}_E \dot{\mathbf{U}}_E - \mathbf{B}_E^T \mathbf{K}_E(t) \mathbf{B}_E \mathbf{U}_E = \mathbf{F}_E \qquad (14)$$

Where $\mathbf{m}_E$ is the element mass matrix and $\boldsymbol{\xi}_E$ the damping.

Considering a single node, say i, the contribution of each element having i as vertex has to be considered, so that the dynamic nodal equilibrium equation has to be re-written, in the most general case as:

$$\left(\sum_{j=1}^{N_E^i}\mathbf{n}_j\mathbf{m}_j\mathbf{n}_j^T\right)\ddot{U}_i+\left(\sum_{j=1}^{N_E^i}\mathbf{n}_j\boldsymbol{\xi}_j\mathbf{n}_j^T\right)\dot{U}_i-\left(\sum_{j=1}^{N_E^i}\mathbf{n}_j\mathbf{B}_E^T\mathbf{K}_E(t)\mathbf{B}_E\mathbf{U}_j\right)=F_i \quad (15)$$

Where:

1. $\mathbf{n}_j$ is a 1×3 unitary vector with $\mathbf{n}_j(k)=1$ if node i for the local internal ordering of element j is equal to k, $\mathbf{n}_j(k)=0$ otherwise;
2. N_E^i is the total number of elements sharing node i;
3. $\mathbf{U}_j$ is a 3×1 vector of displacements of element j vertices.

Within a β-Newmark scheme $\ddot{U}_i$, $\dot{U}_i$ and U_i for each node may be re-written as $\ddot{U}=(1-2\beta)\ddot{U}^{(n)}+2\beta\ddot{U}^{(n+1)}$. When the constant average acceleration method is used, then β=1/4. Assuming γ=1/2, the update rules are the following:

$$\begin{aligned}\dot{U}^{(n+1)}&=\dot{U}^{(n)}+\frac{\Delta t}{2}\left(\ddot{U}^{(n)}+\ddot{U}^{(n+1)}\right)\\ U^{(n+1)}&=U^{(n)}+\Delta t\dot{U}^{(n)}+\frac{1-2\beta}{2}\Delta t^2\ddot{U}^{(n)}+\beta\Delta t^2\ddot{U}^{(n+1)}\end{aligned} \quad (16)$$

Assuming values of $U^{(n)}$, $\dot{U}^{(n)}$ and $\ddot{U}^{(n)}$ at time step n known, the only unknown to determine is the acceleration at step n+1. $\ddot{U}^{(n)}$ is solved by means of the matrix dynamic equilibrium equation, as follows:

$$\begin{aligned}&\left(\sum_{j=1}^{N_E^i}\mathbf{n}_j\mathbf{m}_j\mathbf{n}_j^T\right)\ddot{U}_i^{(n+1)}+\left(\sum_{j=1}^{N_E^i}\mathbf{n}_j\boldsymbol{\xi}_j\mathbf{n}_j^T\right)\left(\dot{U}^{(n)}+\frac{\Delta t}{2}\left(\ddot{U}_i^{(n)}+\ddot{U}_i^{(n+1)}\right)\right)-\\ &-\left(\sum_{j=1}^{N_E^i}\mathbf{n}_j\mathbf{B}_E^T\mathbf{K}_E(t)\mathbf{B}_E\left(\mathbf{U}_j^{(n)}+\Delta t\dot{\mathbf{U}}_j^{(n)}+\frac{1-2\beta}{2}\Delta t^2\ddot{\mathbf{U}}_j^{(n)}+\beta\Delta t^2\ddot{\mathbf{U}}_j^{(n+1)}\right)\right)=F_i\end{aligned} \quad (17)$$

Rearranging the previous equation, we obtain:

$$\begin{aligned}&\left[\left(\sum_{j=1}^{N_E^i}\mathbf{n}_j\mathbf{m}_j\mathbf{n}_j^T\right)+\left(\sum_{j=1}^{N_E^i}\mathbf{n}_j\boldsymbol{\xi}_j\mathbf{n}_j^T\right)\frac{\Delta t}{2}\right]\ddot{U}_i^{(n+1)}-\sum_{j=1}^{N_E^i}\mathbf{n}_j\mathbf{B}_E^T\mathbf{K}_E(t)\mathbf{B}_E\left(\beta\Delta t^2\ddot{\mathbf{U}}_j^{(n+1)}\right)\\ &=F_i-\left(\sum_{j=1}^{N_E^i}\mathbf{n}_j\boldsymbol{\xi}_j\mathbf{n}_j^T\right)\left(\dot{U}^{(n)}+\frac{\Delta t}{2}\ddot{U}_i^{(n)}\right)+\sum_{j=1}^{N_E^i}\left(\mathbf{n}_j\mathbf{B}_E^T\mathbf{K}_E(t)\mathbf{B}_E\left(\mathbf{U}_j^{(n)}+\Delta t\dot{\mathbf{U}}_j^{(n)}+\frac{1-2\beta}{2}\Delta t^2\ddot{\mathbf{U}}_j^{(n)}\right)\right.\end{aligned} \quad (18)$$

Which, assembled for all nodes provides a system of equations on the updated nodal accelerations $\ddot{U}_i^{(n+1)}$ at step n+1.

5 STRUCTURAL APPLICATIONS

In this Section, a structural application on a perforated masonry wall experimentally tested by Vaculik and Griffith [17] is numerically analysed. The experimental work to compare with was conducted at the University of Adelaide, on a series of perforated walls with complex boundary conditions and eventually axial pre-compression, Figure 5. The authors were not able to collect sufficient information from [17] to match exactly experimental results. However, since the aim of the present paper is only to preliminarily show the capabilities of the procedure proposed, the same sinusoidal acceleration applied to the specimens by Vaculik and Griffith [17] is considered. The wall here considered is 1840 mm in length and 1232 mm in height, with an asymmetrically positioned window opening, see Figure 5. The wall was restrained by means of a complex experimental setup,

so that Vaculik and Griffith [17] considered on their models the walls constrained by simple supports at the top and bottom edges and full moment restraint at the vertical edges, with boundary conditions representative of a real situation. The walls were built on concrete slabs, which were lifted together onto the shake-table prior to testing. As shown by Figure 5, the test wall was restrained at the vertical edges by a stiff frame representative of the in-plane stiffness expected for a masonry wall acting in-plane to the seismic excitation. A horizontal cross bar attached to the stiff in-plane frame provided support to the wall at the top edge.

The brick units, cut from clay pavers are in scale ones with 110 × 50 × 39 mm dimensions (length × width × height). Material properties adopted in the model are summarized in Table 2 and they generally agree with those reported in [17], where a wide preliminary characterization of the constituent materials was done. Masonry tensile strength adopted in the model is generally lower than that experimentally determined in single bending tests, however authors experienced an elastic behaviour with higher values of f_t for the model. Finally the adopted elastic modulus of the brick is kept lower than that experimentally determined, i.e. 32100 MPa, with the sole aim of finding the exact elastic modulus experimentally determined for masonry, i.e. 9180 MPa.

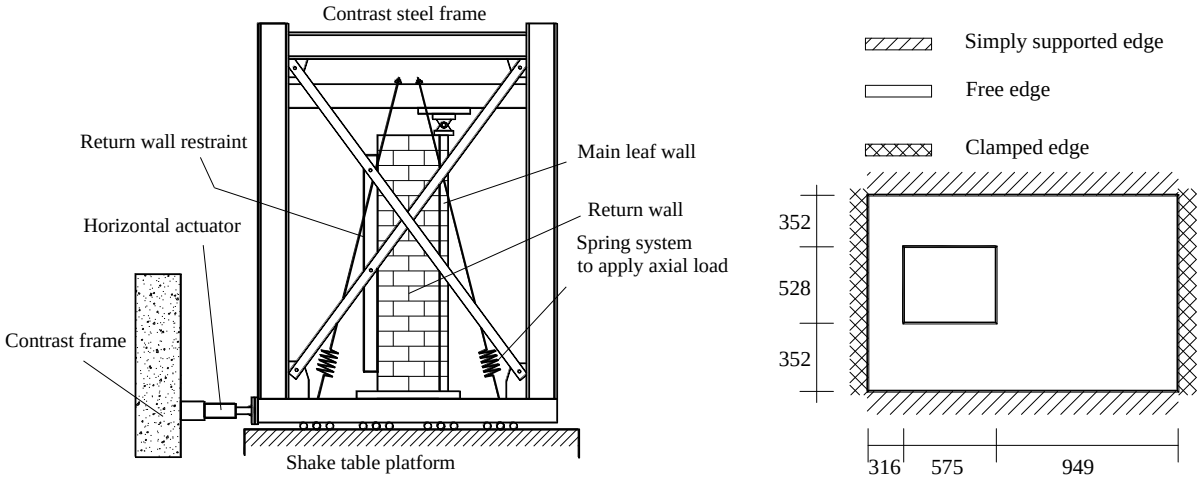

Figure 5: Experimental set-up to perform the dynamic analyses (left) and geometry of the perforated wall (in mm) subjected to the dynamic tests in two way bending (right)

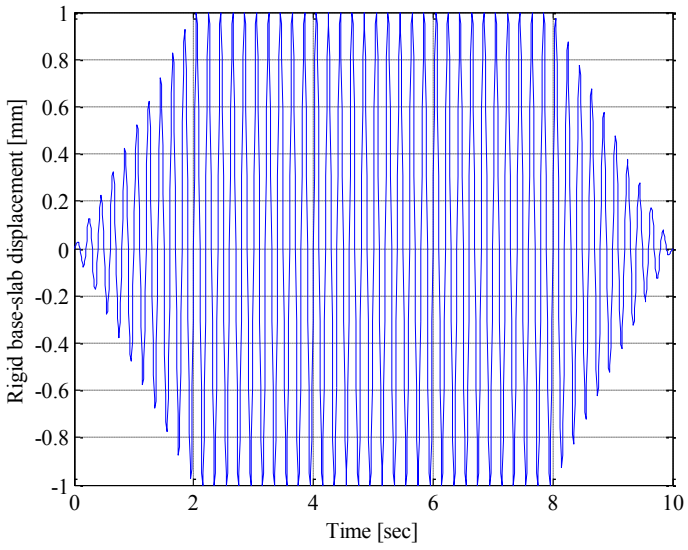

Figure 6: time-displacement law applied to the shake table base

Table 2: Perforated wall subjected to dynamic excitation. Mechanical properties assumed for the constituent materials.

	joint	brick-brick interface	Triangles brick		
E	6000	18000	18000	[MPa]	Young Modulus
G	E/2	E/2	E/2	[MPa]	Shear Modulus
c	1.2 ft	1	-	[MPa]	Cohesion
f_t	0.05	-	-	[MPa]	Tensile strength
f_c	25.9	-	-	[MPa]	Compressive strength
Φ	30	45	-	[°]	Friction angle
Ψ	45	-	-	[°]	Angle of the linearized compressive cap
G_f^I	0.02	10	-	[N/mm]	Mode I fracture energy
G_f^{II}	0.04	10	-	[N/mm]	Mode II fracture energy

The results of the numerical analysis are summarized in Figure 7, where the time-displacement curve of point P and the deformed shape at the end of the simulation process are represented. As can be noted, there is a clear residual displacement (order of magnitude 2 mm) with a formation of a failure mechanisms involved inclined yield lines passing through the corners of the internal window and a vertical yield line on the first row of elements, near the fixed support.

While the approach proposed needs further validation with experimental data (if present) and alternative numerical simulations conducted with both commercial FEM and the distinct element method, the simple procedure proposed in the paper appears quite appealing from a practical point of view, needing very reduced computational time to be performed and being the dynamic analyses fully explicit.

6 CONCLUSIONS

The first preliminary results obtained with a homogenization model for the out-of-plane non-linear dynamic analysis of masonry walls has been presented. The model requires an initial non-linear homogenization with softening materials and a coarse FE discretization of the unit cell. The structural implementation is done within a Kirchhoff-Love thin plate hypothesis and with a discretization with rigid triangular elements and non-linear homogenized interfaces exhibiting deterioration of the mechanical properties and possible energy dissipation only for flexural actions.

The dynamic problem is particularly simple, explicit and requires very few kinematic variables to be solved under any input accelerogram.

The code is preliminary tested on a windowed panel subjected to a sinusoidal excitation and already experimentally tested at the University of Adelaide under different levels of pre-compression and dynamic excitation.

REFERENCES

[1] Corradi, M.; Borri, A.; Vignoli, A.: Strengthening techniques tested on masonry structures struck by the Umbria–Marche earthquake of 1997–1998. *Construction and Building Materials,* 16 (2002) 4, 229-239.

[2] Doglioni, F.; Petrini, V.; Moretti, A. (Eds) (1994). Le chiese e il terremoto [Churches and earthquake]. LINT press, Trieste, Italy.

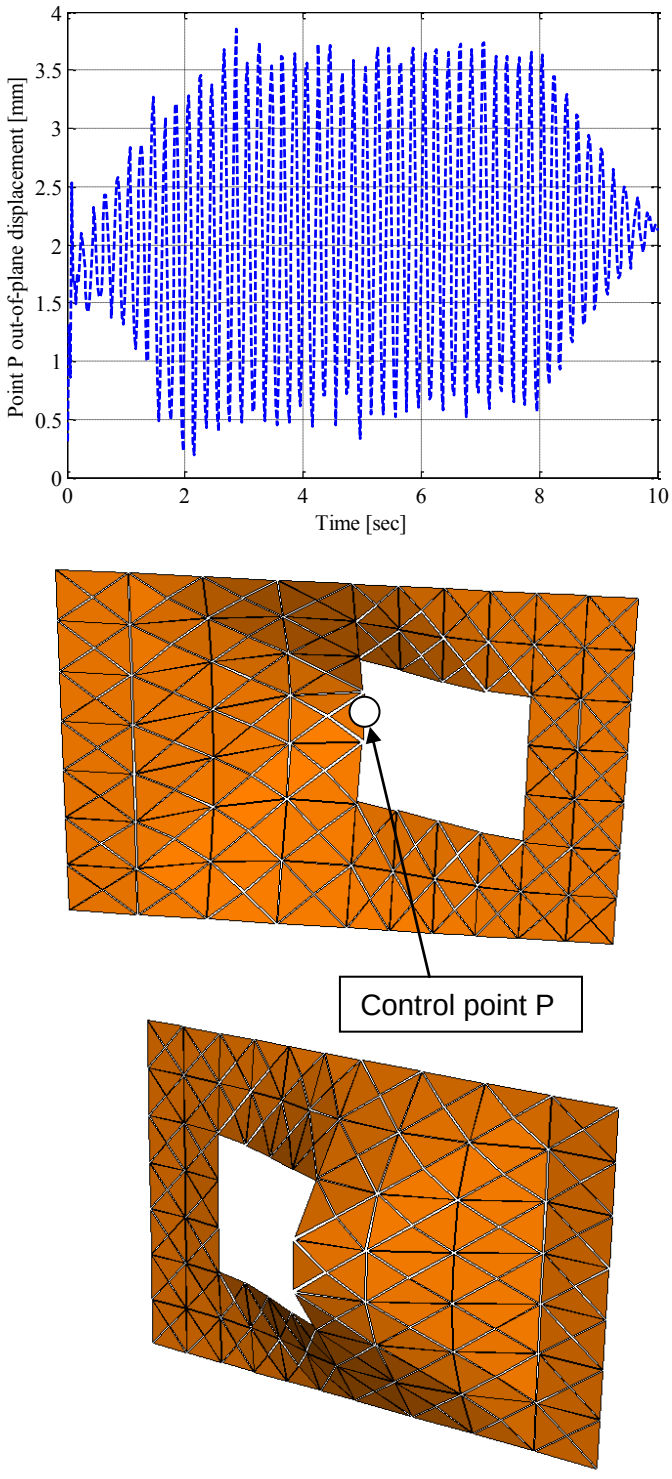

Figure 7: Time-displacement history of point P (corner of the window) and final deformed shape configuration of the wall.

[3] Corradi, M.; Borri, A.; Vignoli, A.: Strengthening techniques tested on masonry structures struck by the Umbria–Marche earthquake of 1997–1998. *Construction and Building Materials,* 16 (2002) 4, 229-239.

[4] Doglioni, F.; Petrini, V.; Moretti, A. (Eds) (1994). Le chiese e il terremoto [Churches and earthquake]. LINT press, Trieste, Italy.

[5] Pietruszczak, S.; Ushaksarei, R.: Description of inelastic behaviour of structural masonry. *Int J Solids Struct*, 40 (2003), 4003–19.

[6] Lourenço, P.B.; Rots, J.: A multi-surface interface model for the analysis of masonry structures. *Journal of Engineering Mechanics ASCE,* 123 (1997) 7, 660-668.

[7] Lourenço, P.B.; de Borst, R.; Rots, J.G.: A plane stress softening plasticity model for orthotropic materials. *International Journal for Numerical Methods in Engineering*, 40 (1997), 4033-4057.

[8] Luciano, R.; Sacco, E.: Homogenisation technique and damage model for old masonry material. *International Journal of Solids and Structures*, *34* (1997) 24, 3191-3208.

[9] Massart, T.; Peerlings, R.H.J.; Geers, M.G.D.: Mesoscopic modeling of failure and damage-induced anisotropy in brick masonry. *Eur J Mech A/Solids*, 23 (2004), 719–35.

[10] Milani, G.; Tralli, A.: Simple SQP approach for out-of-plane loaded homogenized brickwork panels, accounting for softening. *Computers and Structures*, 89 (2011), 201–215.

[11] Gambarotta, L.; Lagomarsino, S.: Damage models for the seismic response of brick masonry shear walls. Part II: The continuum model and its applications. *Earthquake Engineering and Structural Dynamics*, 26 (1997) 4: 441-462.

[12] Munro, J.; Da Fonseca, A.M.A.: Yield-line method by finite elements and linear programming. *J. Struct. Eng. ASCE*, 56B (1978), 37-44.

[13] Milani, G.; Lourenço, P.B.; Tralli, A.: Homogenised limit analysis of masonry walls. Part I: failure surfaces. *Computers & Structures*, 84 (2006) 3-4,166-180.

[14] Van der Pluijm, R.; Rutten, H.S.; Schiebroek, C.S.: Flexural behaviour of masonry in different directions. In: *Proc. 4th Int. Masonry Conf.,* Brit. Mas. Soc. 1992, 117-123.

[15] Van der Pluijm, R.: *Out-of-plane bending of masonry. Behavior and strength,* PhD Thesis: Eindhoven University of Technology, The Netherlands 1999.

[16] Lourenço, P.B.: Aspects related to the out-of-plane numerical modelling of masonry. Masonry International, 14 (2000) 1, 31-34.

[17] Vaculik, J.; Griffith, M.: Shaketable tests on masonry walls in two-way bending. In: *Proc. AEES 2007 Conference*, Australian Earthquake Engineering Society, Nov. 2007, Wollongong, Aust.

[18] Vaculik J.: Unreinforced masonry walls subjected to out-of-plane seismic action. PhD Thesis, University of Adelaide, Australia 2012.